UCRL-ID-134280

Comparisons of Cloud Covers and Cloud Fractions Using Remote-Sensing Retrievals

D.J. Rodriguez
S.K. Krueger

May 18, 1999

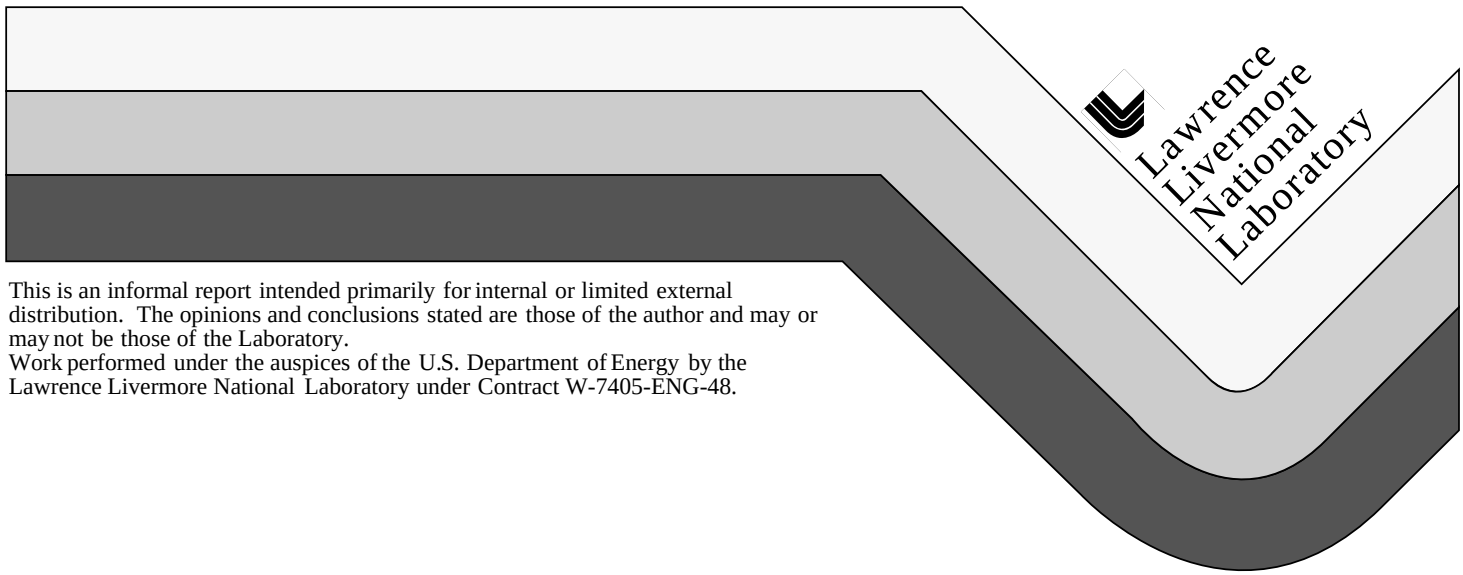

Comparisons of Cloud Covers and Cloud Fractions Using Remote-Sensing Retrievals

Daniel J. Rodriguez
Atmospheric Science Division
Lawrence Livermore National Laboratory
Livermore, CA

Steven K. Krueger
Department of Meteorology
University of Utah
Salt Lake City, UT

1. Introduction

The DOE's Atmospheric Radiation Measurement (ARM) Program employs both upward- and downward-looking remote-sensing instruments to measure the horizontal and vertical distributions of clouds across its Southern Great Plains (SGP) site. No single instrument is capable of completely determining these distributions over the scales of interest to ARM's Single Column Modeling (SCM) and Instantaneous Radiative Flux (IRF) groups; these groups embody the primary strategies through which ARM expects to achieve its objectives of developing and testing cloud formation (USDOE, 1996). Collectively, however, the data from ARM's cloud-detecting instruments offer the potential for such a three-dimensional characterization.

Data intercomparisons, like the ones illustrated here, are steps in this direction. Specifically, they are valuable because they help: provide a measure of uncertainty in ARM's measurement capabilities, calibrate retrieval methods and refine algorithms and concepts. In the process, we are forced to think of meaningful ways in which measurements from different instruments can be compared and, perhaps, combined. While the ultimate goal of this particular effort is to develop the ability to accurately characterize cloud fields in three dimensions over time at the SGP site, along the way we will address such questions as "which source, or combination of cloud data sources, offers a 'best estimate' product?" and "how can cloud observations be used to evaluate the representation of clouds in numerical models?". Examples of some initial comparisons, involving satellite, millimeter cloud radar, whole sky imager and ceilometer data, are provided herein.

2. Cloud Detection

A sizable array of instrumentation, designed specifically for the remote sensing of cloud properties, has been deployed around ARM's Cloud and Radiation Testbed (CART) site in north-central Oklahoma and south-central Kansas (Fig. 1). Besides the acquisition of data from ground-based, *in situ* instruments, NASA's Langley Research Center has analyzed GOES-8 radiance data to derive cloud properties across the Southern Great Plains at times that correspond to ARM's Intensive Observation Periods (IOPs). Some basic features of the instruments whose data we highlight in this study are now described.

- The Whole Sky Imager (WSI) is a passive, automated system for measuring the sky radiance in approximately 0.3 ^{o} increments over the entire sky dome (Shields, et al., 1990). Red, blue, infrared and neutral images are routinely acquired once every 10 minutes. For daytime data, an algorithm ratios the red and blue images and compares the result, on a pixel-by-pixel basis, to a matching clear sky image, extracted from a library of images that cover the range of solar zenith angles. (A soon-to-be-released daytime algorithm will perform radiometric calibrations that will eliminate the need for background data.) A pixel is cloudy whenever the test image ratio exceeds the background ratio by a specified amount. The principal derived quantity is cloud amount, which the algorithm estimates by summing the number of cloudy pixels and dividing the result by the total number of pixels.

- The Micropulse Lidar (MPL) is a zenith-pointing, optical remote sensing system designed primarily to determine the altitude of clouds overhead (Spinhirne, et al., 1995). It transmits pulses of energy and then measures the backscattered signal in 300-meter range bins, up to about 20 kilometers. Analysis of the backscatter profile, obtained from 60-second averages, with a threshold algorithm provides the lowest cloud base height in kilometers. The system, which is highly sensitive, is capable of detecting both visible clouds and sub-visible cirrus.

- The Belfort Laser Ceilometer (BLC), like the MPL, is a ground-based, optical remote sensing instrument. Clouds are detected by transmitting pulses of infrared light vertically into the atmosphere, and then measuring the scattered light from clouds and precipitation with a receiver telescope. The primary quantities measured by this system are the base heights of the lowest, second lowest and third lowest clouds, up to 7625 meters over 7.6-meter range gates. The current default rate for data acquisition is 30 seconds.

- ARM's Millimeter Cloud Radar (MMCR) maps the vertical distributions of all types of clouds whose reflectivities, resulting from the radar's electromagnetic pulses, range from approximately –50 dBZ to 20 dBZ (Clothiaux, et. al., 1998). The breadth of this range is achieved by using four distinctly different operational modes which, when the four sets of corresponding data are combined, produces an accurate depiction of clouds in the vertical column above the radar every 36 seconds. Besides providing

information on the microphysical structure of non-precipitating clouds, the use of masking routines allows cloud boundary heights to be determined within 90 meters of their true value.

- NASA's Geostationary Operational Environmental Satellite (GOES-8) passively measures visible and infrared radiances, nominally every half hour (Minnis and Smith, 1997). The radiances, along with surface-based temperature observations, are used to derive cloud properties, including cloud amount, height and thickness over a 3x3 grid, having a 0. 3 ^{o} resolution, and over a 20x28 grid, having a 0.5 ^{o} resolution, during ARM's IOPs; both grids are centered on the Central Facility. The pixel resolution within each cell is approximately 4 kilometers. Pixels are cloudy or clear depending on the prevailing radiance threshold.

Table 1 identifies all of ARM's remote-sensing, cloud-detecting instruments (whether utilized in this study or not), their location within the CART network, and the products currently derived from their data. The reader should refer to Fig. 1 for the locations of ARM's Central Facility (CF), four Boundary Facilities (BF) and 23 Extended Facilities (EF).

3. Data Intercomparisons

The variety of ARM instrumentation is greatest at the CF cluster. Given that more opportunities for data intercomparison exist at the CF, our attention has been focused there with the expectation that many of the lessons learned can later be adapted to cloud data at the BFs, and perhaps across the entire CART domain. Principally, we are concerned about: 1) the accuracy of various estimates of cloud properties at a single point, or within a thin vertical column, above the CF over time, and 2) the accuracy of various estimates of cloud properties over the CART site, which can then be reduced to single, representative profiles over time. In the former case, the results are usable in the IRF and SCM strategies; in the latter case, they satisfy SCM needs specifically. All cloud products described below fit within one of these categories.

3a. Cloud Fractions from WSI and Combined MPL-BLC Data at the Central Facility

The sky imager and ceilometer data used in this particular study were collected at the SGP Central Facility between October 1 and December 31, 1996. This three-month period, corresponding to the first set of WSI data released by ARM's Experiment Center, was sufficiently long to reveal important trends (Rodriguez, 1998). Comparisons were made by invoking the ergodic assumption, whereby ensemble, time and space averages are assumed to be equivalent. Hourly values of cloud fraction from WSI data were formed by averaging six cloud fraction estimates, all gathered within 10 degrees of zenith, from 10-minute images. A corresponding ceilometer estimate was formed by dividing the cloud detections by the total number of measurements, typically 60, over the same hour. Use of MPL or BLC data in defining the cloud occurrence frequency (COF) over an

hour's time depended on the cloud base height; it is generally acknowledged that the BLC is best at detecting clouds in the 0-3000 meter range, while the MPL has greater sensitivity at higher altitudes (Turner, 1990).

The scatter of points in Fig. 2, based on temporal pairings of the WSI and ceilometer cloud fractions, reveals the relationship between these data. In particular, the points aligned along the ordinate, which correspond to clear (WSI) and varying cloudy (ceilometer) combinations, show the poor correlation between these paired-in-time data. Inspection of many associated data records confirms that the WSI algorithm often produces cloud fraction estimates of zero, while the MPL, with its greater sensitivity, reports the presence of thin or sub-visual cirrus. (Biases to this degree should diminish with the new WSI daytime algorithm.) To demonstrate that the correspondence between the hourly WSI and ceilometer comparisons deteriorates as a function of range, the cumulative frequencies of the absolute differences of the ceilometer and WSI cloud fractions in low (< 2000 meter), middle (2000 – 5000 meter) and high (> 5000 meter) cloud layers are plotted in Fig. 3. Given the conservative definition of a cloud, as used by the WSI decision algorithm, it is not surprising that the best agreements occur for low cloud bases. Within this category, 35% of the paired values agree exactly and 75% of the values agree within plus or minus 10%. However, the correspondence decays with increasing cloud base height until it becomes uncorrelated at 5000 meter and beyond.

3b. Cloud Amounts from Local (0.3 º) GOES-8 and MPL Data at the CF

Cloud amounts over ARM's Central Facility, based on measurements of radiance by the GOES-8 radiometer and analyses by NASA's Langley Research Center (LaRC) on a 3x3 grid, are compared in Fig. 4 against hourly, time-centered COFs derived from MPL data. The time line, expressed in Julian days, spans the July 1995 SCM IOP, which the SCM group refers to as Case 1. The red-filled areas correspond to times at which the satellite estimates exceed the MPL estimates; the green-filled areas represent the converse situation. Overall, the agreement is good, but red clearly dominates the scene. Analyses of the satellite data, which are sometimes referred to as Minnis products, suggest that the skies tend to be clear or overcast, while detections by the MPL suggest a higher frequency of scattered and broken clouds. Possible reasons for these discrepancies are explored momentarily.

3c. Diurnal Averages of Cloud Amounts from Local GOES-8 and MPL Data at the CF

One way of quantifying the biases noted in the Fig. 4 is to calculate and compare the time-mean cloud amounts from the satellite and MPL data over the July 1995 SCM IOP. (The Langley group analyzed six more days of satellite data, three on either side of the actual IOP; these additional analyses have been incorporated into the study, thereby extending the period to 24 days.) Occasionally, one or

both instruments were inoperative, leading to averages composed of as few as 15 values and as many as 23 values. The results in Fig. 5 split naturally into two groups. During the nighttime, the cloud cover estimates from MPL data generally exceed the estimates from satellite data, but only slightly; conversely, during the daytime, the GOES-8 estimates always exceed the MPL estimates by a sizable amount. Both sets of curves track one another reasonably well, suggesting that the same cloud fields are being observed, but interpreted somewhat differently.

The results were unexpected for two reasons. First, the nighttime comparisons are surprisingly good given that nighttime analyses are based on radiances from a single (11 micron) channel and a simple threshold technique. The method often performs poorly when clouds are low or thin because of the lack of a temperature contrast between these clouds and the clear surface. This occurs because of LaRC's use of surface air temperature as a predictor for the TOA clear sky temperature in the evening, which can lead to clear skies being erroneously identified as cloudy. However, a plot of cloud fractions (not shown), generated from satellite data as a function of time and height, showed thick clouds at heights that varied between 4 and 12 kilometers above the ground, when clouds were present. Apparently, the contrasts were sufficiently large to produce reasonable estimates of cloud amount during the nighttime. Second, the bias between the MPL and GOES-8 results during the daytime (with the MPL data suggesting lesser cloud amounts) is surprisingly large, especially considering the MPL's documented sensitivity to high, thin cirrus.

Thus far, three plausible explanations for these results have surfaced, none of which are necessarily exclusive or correct. One obvious explanation would be that the signal returned to the MPL receiver was severely affected by solar contamination. However, the outcome of the WSI and ceilometer data comparisons would suggest otherwise. Next, upon checking with the designers and builders of the MPL, we discovered that in July 1995 the laser was operating at half its current power of 1 W, meaning that the return signal was about an order of magnitude less than its current strength. In other words high, optically thin clouds may have escaped detection by the MPL, leading to under-estimations of cloud amount. Lastly, the bi-spectral (0.63 and 11 micron) threshold technique being applied to the GOES-8 radiance data during the daytime may tend to over-represent cloudiness due, perhaps, to difficulties in specifying clear sky radiances. This latter possibility is explored more extensively in the following section.

3d. Diurnal Cloud Amounts based on GOES-8 and MPL "Pixel" Data

For one of our Case 1 studies, the satellite product used is based on radiance data collected within a 0.3 ^{o} box, centered over the CF and comprised of approximately 60 pixels. The pixels are either clear or overcast depending on thresholds determined as functions of scene type, solar and satellite viewing angles, and clear sky radiances. The cloud amount is simply the fraction of

overcast pixels within the grid box. For purposes of comparison, we "mimic" the satellite data, using MPL data, in accordance with the following arguments. If the pixel resolution is dx and the mean wind speed at cloud height is u, then a pixel will traverse the MPL sampling space in time interval dt = dx/u. If the mean wind speed is 10 meters/second, a "conservative" cloud element travels 40 kilometers, or roughly 0.3 ^{o}, in about one hour. If, as in the previous analyses, we retain the one-hour window for the MPL data, centered on the satellite observation time, and if we assume that the MPL "pixels" are 4 kilometers wide, corresponding to the pixel resolution of the GOES-8 radiometer, there will be 10 cloud characterizations per hour, i.e., dt will equal 6 minutes. While the resulting resolution is admittedly coarse (cloud amounts over an hour's time become multiples of 10% for MPL data averaged over one minute), the characterizations are not believed to be overly restrictive when diurnal composites are formed over 24 days.

With these conditions and assumptions in effect, we defined an MPL "pixel" as being overcast in three different ways:

1. A cloud is detected by the MPL at least once during time interval dt;
2. Clouds are detected at least half the time during time interval dt; and
3. Clouds are always present during time interval dt.

The curves and points labeled thresh_1, thresh_half and thresh_all in Fig. 6 correspond, respectively, to cloud definitions 1, 2 and 3 above. During the daytime, thresh_1 matches the diurnally-averaged satellite cloud amounts best, while during the nighttime thresh_all is best. The nighttime result may indicate that the IR threshold scheme in use at the time of the analyses had difficulty distinguishing low cloud tops from the ground surface. (Note that an earlier statement about clouds being present between 4 and 12 kilometers does not preclude the existence of low clouds, i.e., cloud heights derived from satellite data represent composite heights whenever multiple layers are present.) Lastly, a comparison of these results against the time series of MPL and GOES-8 cloud amounts in Fig. 4 suggests that the apparent overestimation in the frequency of overcast conditions, as derived from satellite data, occurred during periods of scattered and broken clouds, as registered by the lidar.

3e. GOES-8 Cloud Amounts Over the CART Site and Over the CF

ARM cloud researchers have an interest in knowing the extent to which the cloud cover over a limited area represents cloudiness over a much broader area. Fig. 7 compares the 0.3 ^{o} Minnis cloud amounts over the CF (the cell is roughly 40 kilometers squared) to the averages of a 5x5 subset of the 0.5 ^{o} cloud amounts, whose area approximately matches the horizontal dimension of an SCM column, during the July 1995 SCM IOP. The information is presented in a format identical to the one used previously in Fig. 4. There are few surprises. Over the smaller area, the cloud amounts tend to be binary, i.e., the skies are either clear or overcast; while changes in the mesoscale cloud amounts, when they occur, tend

to be more gradual. In other words, a greater incidence of scattered and broken clouds can be seen in averages over the larger grid.

3f. Average GOES-8 Cloud Fractions Over the CART Site and MMCR

Cloud Fractions over the CF

Representative profiles of cloud fractions over time at the SGP site are valued by the SCM group as they provide important statistics against which a particular set of model results can be compared. The data stream from which this product is derived resides in the 0.5 ^{o} GOES-8 file. It contains cloud amounts, cloud top heights and cloud thicknesses at levels that correspond to low (< 2000 meters), middle (2000–6000 meters) and high (> 6000 meters) cloud layers on a 20x28 grid. Using the same 5x5 subset as above, 25 individual profiles of cloud occurrence were constructed at regular, vertical (250 meter) intervals up to 15 kilometers by assigning a value of one to grid points within a cloud and a value of zero to those without, and by multiplying the profile values within the cloud layers by the appropriate cloud amounts. Cloud amounts were then averaged at each vertical grid level. These steps were repeated for each new data time and were followed, if necessary, by linear interpolations every two hours. The resulting time-height arrays of cloud fractions (our definition excludes overlap assumptions) were then contoured and color-filled. The results of this exercise for the second half of the Summer 1997 SCM IOP, also known as SCM Case 3, are shown in Fig. 8. The absence of cloud thickness analyses precludes plotting during the nighttime (the first half of each Julian day).

Similar, but less complicated, procedures were used in deriving cloud fractions for the MMCR data, as shown in Fig. 9. The MMCR data records are more intact, giving us a nearly continuous view of cloudiness over the Central Facility. The smoothing effects of spatial averaging are evident in the previous figure; in contrast, the gradients between clear and cloudy skies in the MMCR plot are more pronounced. Generally, though, the picture that emerges when comparing Figs. 8 and 9 is fairly consistent. Both instruments show the presence of clouds at about the same time, and cloud top heights are comparable; however, the heights of cloud bases rarely agree. There are several possible reasons. The downward-sensing radiometer cannot discriminate between single- and multi-layer clouds, i.e., the instrument measures the composite effects of radiating clouds along a viewing path, so there may be a tendency for overestimating the lowest cloud-base height. On the other hand, the signal from the upward-sensing MMCR is susceptible to contamination by insects and precipitation, i.e., the shafts that reach the ground in Fig. 9 are indicative of a rain event or insects in the boundary layer, both of which can severely attenuate the radar signal and mask the true cloud base. Other researchers have employed more rigorous, value-added procedures for identifying cloud boundaries than were used here.

4. Discussion

Collecting measurements at the SGP and other ARM sites over long periods of time and for a variety of weather conditions is critical to the formation and testing of parameterizations for GCMs, a primary programmatic objective of ARM. The principal means of collecting cloud data, which supports one aspect of this objective, is by remote sensing. Often, measurements and products derived from these measurements provide a unique, if uncertain, resource; for example, the estimation of some cloud macrophysical features across the CART site, as offered by NASA Langley's analyses of satellite radiance data, is comprehensive in its horizontal coverage, but it remains to be seen whether their cloud height analyses are sufficiently and routinely accurate for purposes of model testing. Other instruments, like the millimeter-wavelength cloud radar in combination with ceilometers, use active sensing to penetrate clouds and provide information on their heights and structures, but only in an atmospheric column directly above the radar, i.e., the sampling volume lacks the breadth of spatial coverage that instruments, like satellite-mounted radiometers, can offer. Over time, best-estimate data and data products will emerge from investigations like the ones described in this paper.

Exploratory data analysis techniques have been used effectively in this study to: elicit insights from ARM's cloud datastreams, begin to uncover the structure of clouds, and test underlying assumptions. Through such means we have identified issues of accuracy that need to be addressed. We have found, for example, that the whole sky imager's ability to detect clouds diminishes as a function of range because of a conservative definition of a cloud in the WSI's decision algorithm; we fully expect that remedial actions, recently taken by the WSI mentor, will improve the correspondence between the WSI and MPL estimates of cloud amount in future studies. Still, the fundamental definition of a cloud remains elusive. We have discovered that the definition depends on the resolving power of the instrument, e.g., does it actively or passively sense the atmosphere, and on the techniques used for detection. Clouds whose equivalent, horizontal dimensions are less that 4 kilometers would seemingly constitute sub-grid phenomena to satellite pixels, but they are sizable targets to radars and lidars. However, diurnal composites of cloud amount during the SCM IOP in July 1995 showed a distinct bias, suggesting a more liberal definition of cloudiness when applied to satellite data analysis as compared to the simpler cloud occurrence frequency method used in the MPL data analysis. All of these findings point clearly to the need for additional data intercomparisons.

References

Clothiaux, E.E., K.P. Moran, B.E. Martner, T.P. Ackerman, G.G. Mace, T. Uttal, J.H. Mather, K.B. Widener, M.A. Miller and D.J. Rodriguez, 1998: The Atmospheric Radiation Measurement Program Cloud Radars: Operational Modes. *J. Atmos. Oceanic Technol.,* Accepted.

Minnis. P., and Smith, W.L., Jr.: Cloud and Radiative Fields Derived from GOES-8 During SUCCESS and the ARM-UAV Spring 1996 Flight Series, *Geophys. Res. Ltrs., 25,* April 15, 1998, pp. 1113-1116.

Rodriguez, D.J., 1998: On the Comparability of Cloud Fractions Derived from Whole Sky Imager and Ceilometer Data, Lawrence Livermore National Laboratory Report UCRL-ID-129829.

Shields, J.E. T.L. Koehler, M.E. Karr and R.W. Johnson, 1990: Automated Cloud Cover and Visibility Systems for Real Time Applications. University of California, San Diego, Scripps Institution of Oceanography, Marine Physical Laboratory, Optical Systems Group Technical Note No. 217.

Spinhirne, J.D. J.A.R. Rall, and V.S. Scott, 1995: Compact Eye Safe Lidar Systems**,** *Rev. Laser Eng., 23*, 112-118.

Turner, D.D., 1996: Comparisons of the Micropulse Lidar and the Belfort Laser Ceilometer at the Atmospheric Radiation Measurement Southern Great Plains Cloud and Radiation Testbed Site, Proceedings of the Sixth Atmospheric Radiation Measurement (ARM) Science Team Meeting, San Antonio, Texas, 4-7 March. U.S. Department of Energy, Washington, D.C.

United States Department of Energy, 1996: Science Plan for the Atmospheric Radiation Measurement Program (ARM), DOE/ER-0670T, Washington, D.C.

Work performed under the auspices of the U.S. Department of Energy by Lawrence Livermore National Laboratory under Contract W-7405-ENG-48.

Table 1. Availability of ARM cloud products at the SGP site as a function of facility (Central, CF; Boundary, BF; Extended, EF) and instrument. The spatial coverage of the products increases from left (CF) to right (EF). Entries are made for instruments used during SCM IOPs. Those cloud products enclosed within triple lines are important for calculating gradient quantities and for specifying SCM boundary conditions.

Cloud Products	**Spatial Extent** (⟶ increasing density)		
	CF	BF	EF
Cloud cover	WSI MMCR[#] MPL / BLC[#] GOES-8[*] SIROS / SIR	GOES-8[*] SIROS / SIRS	GOES-8[*] SIROS / SIRS
Cloud base height	MMCR GOES-8[*] MPL BBSS BLC VCEIL	GOES-8[*] BBSS VCEIL	GOES-8[*]
Cloud fraction profile	MMCR GOES-8[*] MPL BBSS	GOES-8[*] BBSS	GOES-8[*]
LWP, r_e average[+]	MWR GOES-8[*]	MWR GOES-8[*]	GOES-8[*]
LWC profile,	MMCR+MWR		

r_e profile[+]			
IWP, d_e layer average[!]	AERI GOES-8[*]	AERI GOES-8[*]	GOES-8[*]
IWC profile, d_e profile[!]	MMCR+AERI		

[*] grid estimates at 0.3 [o] and 0.5 [o] resolution, centered on the CF

[#] cloud occurrence frequency

[+] effective radius of cloud droplet

[!] mean width of ice crystal, weighted by the cross-sectional area

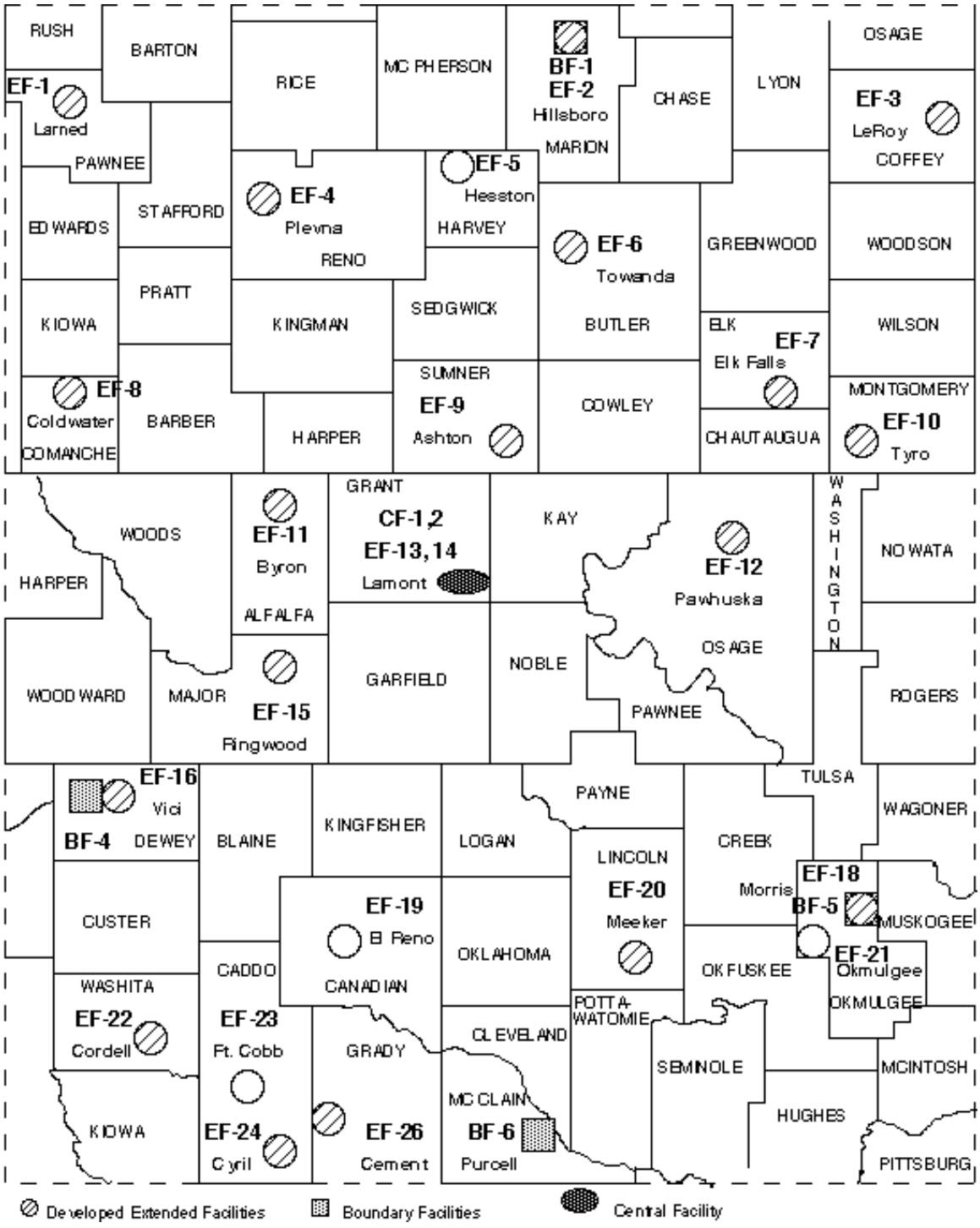

Figure 1. Map of ARM's Southern Great Plains Cloud and Radiation Testbed, showing the locations of the Central, Boundary and Extended Facilities (CF, BF and EF, respectively) that have instruments for remotely sensing the atmosphere.

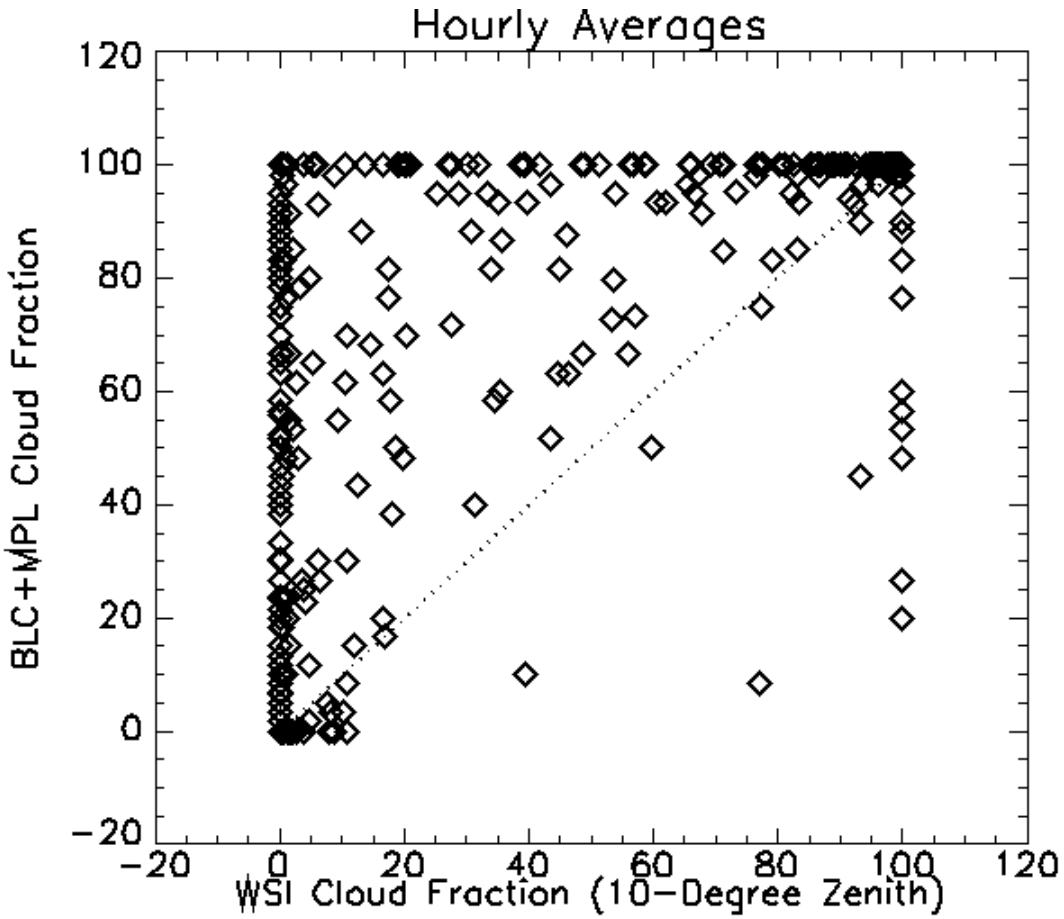

Figure 2. Scatter diagram of the hourly, paired-in-time cloud fractions from the 10 ^{o} WSI and merged BLC and MPL data at the SGP Central Facility over the Fall months of 1996.

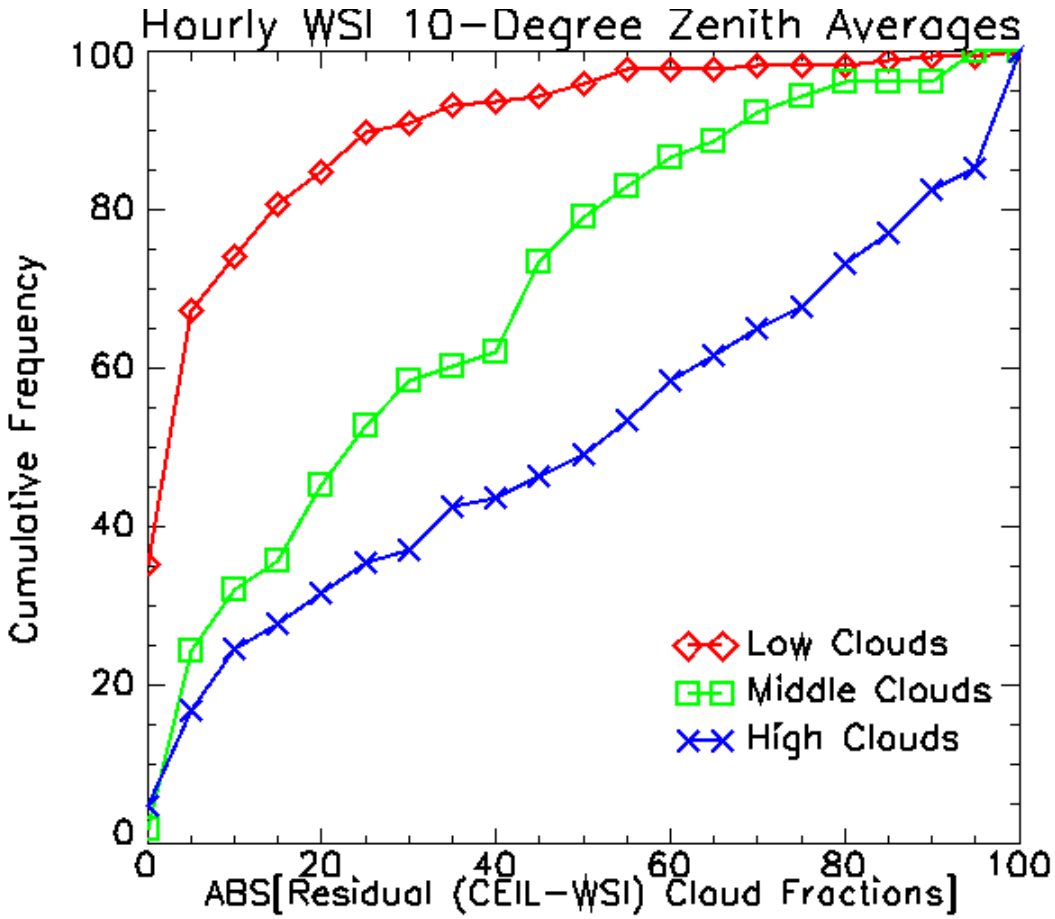

Figure 3. Cumulative frequencies of the absolute differences of the blended ceilometer and 10 ° WSI cloud fractions for cloud base heights in the low-, middle- and high-cloud categories.

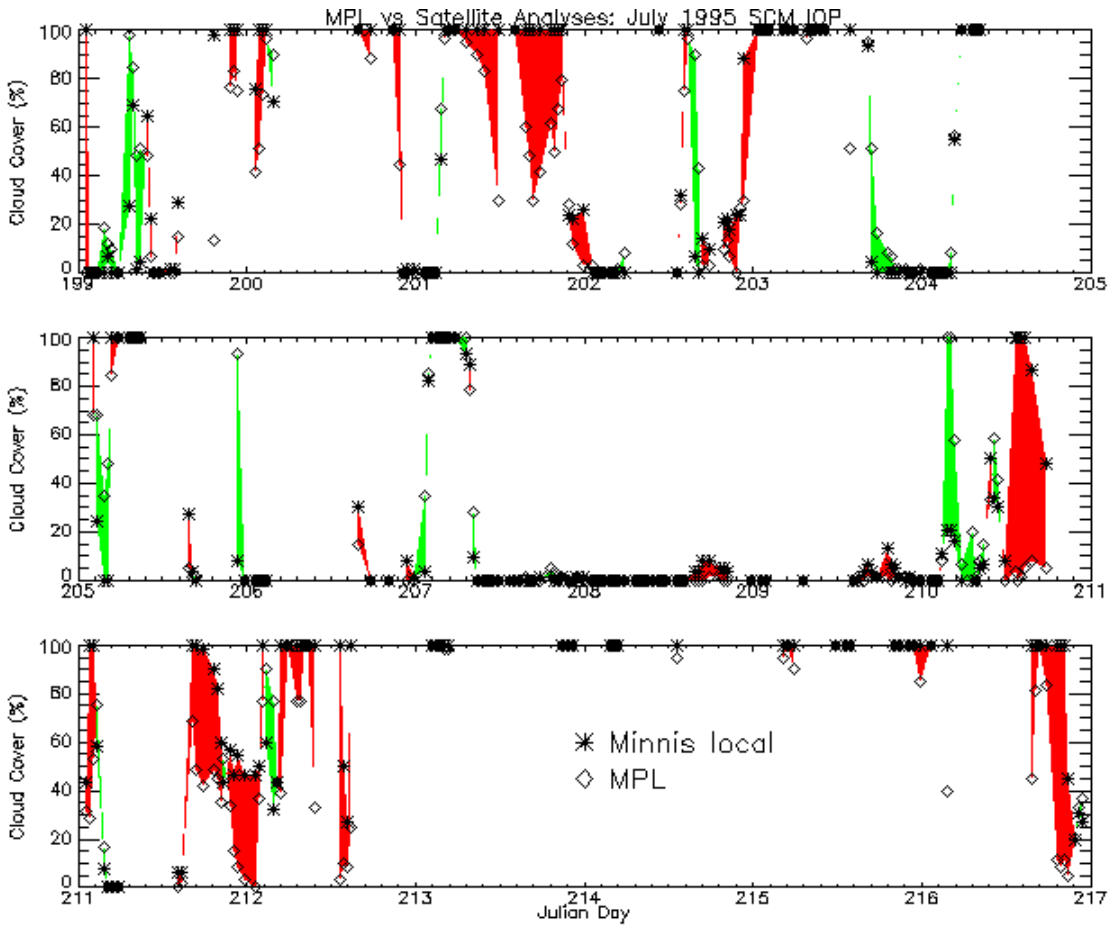

Figure 4. Comparison of cloud covers from the Minnis analyses of GOES-8 0.3 ° (~ 60 pixels) radiance data over the SGP CF and cloud occurrence frequencies from the MPL time-centered, hourly-averaged data during the July 1995 SCM IOP.

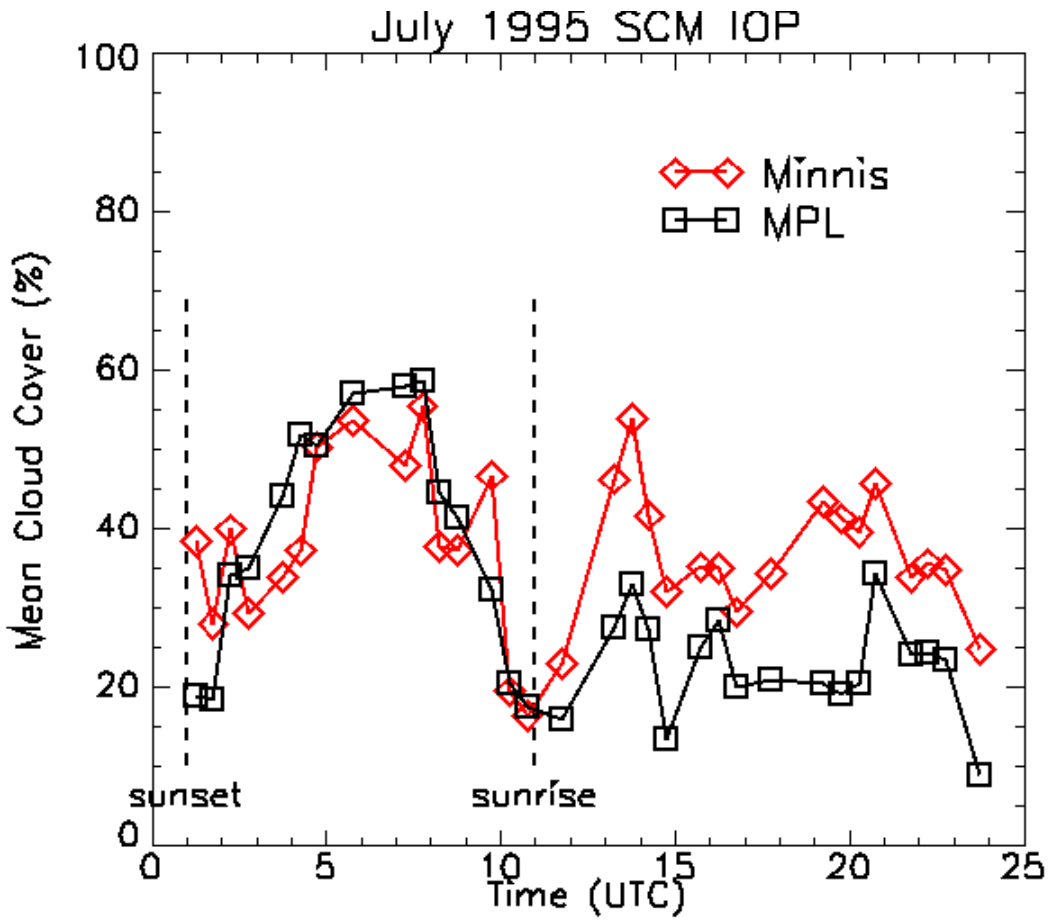

Figure 5. Diurnal composites of cloud amounts over the SGP CF as estimated from MPL and Minnis local (0.3 º) satellite data during the July 1995 SCM IOP.

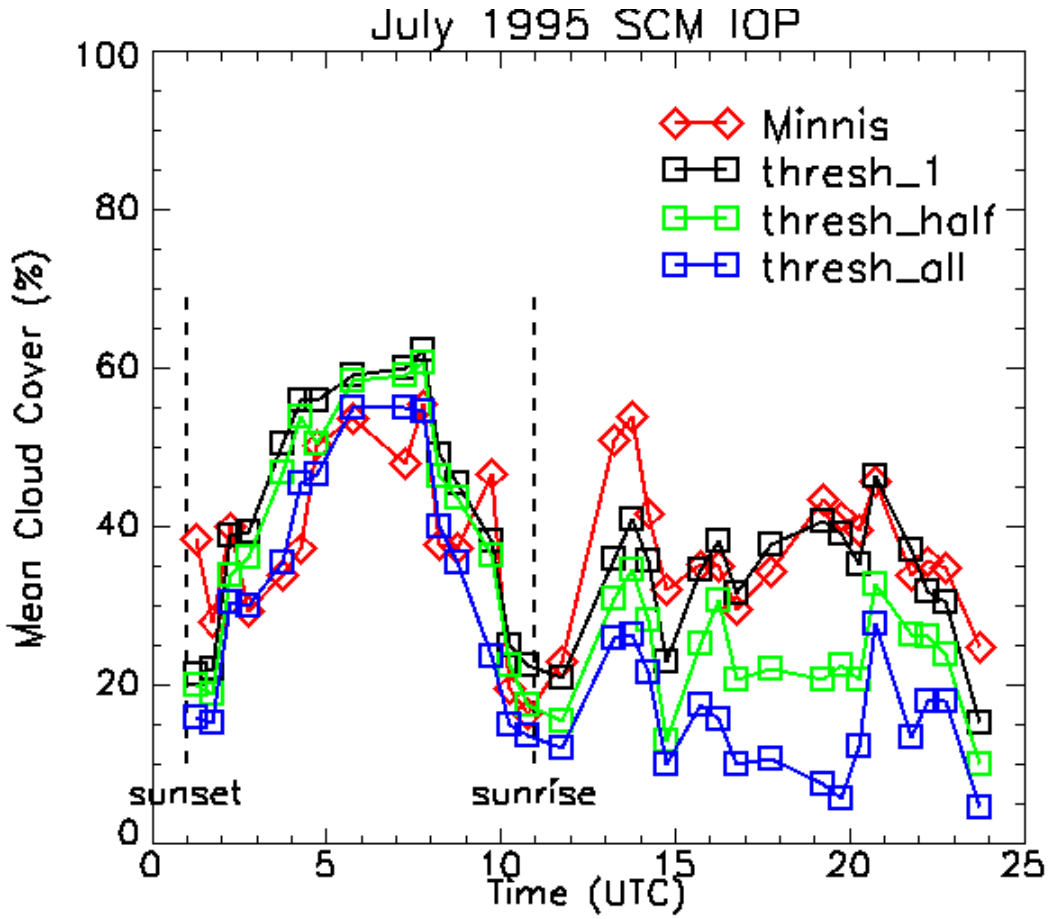

Figure 6. Diurnal cloud amounts over the SGP CF based on local GOES-8 and MPL “pixel” data from the July 1995 SCM IOP.

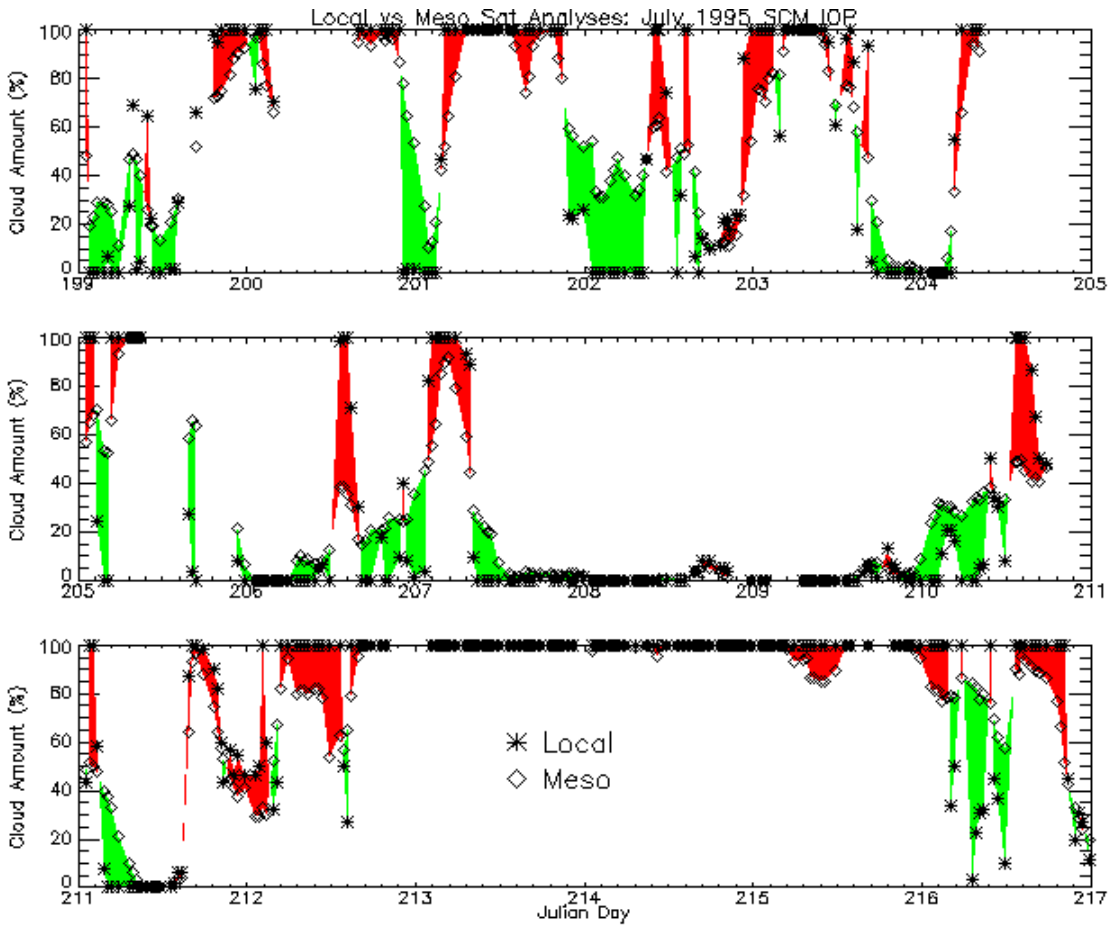

Figure 7.Comparison of satellite cloud covers at the Central Facility and composite cloud covers over the CART site during the July 1995 SCM IOP.

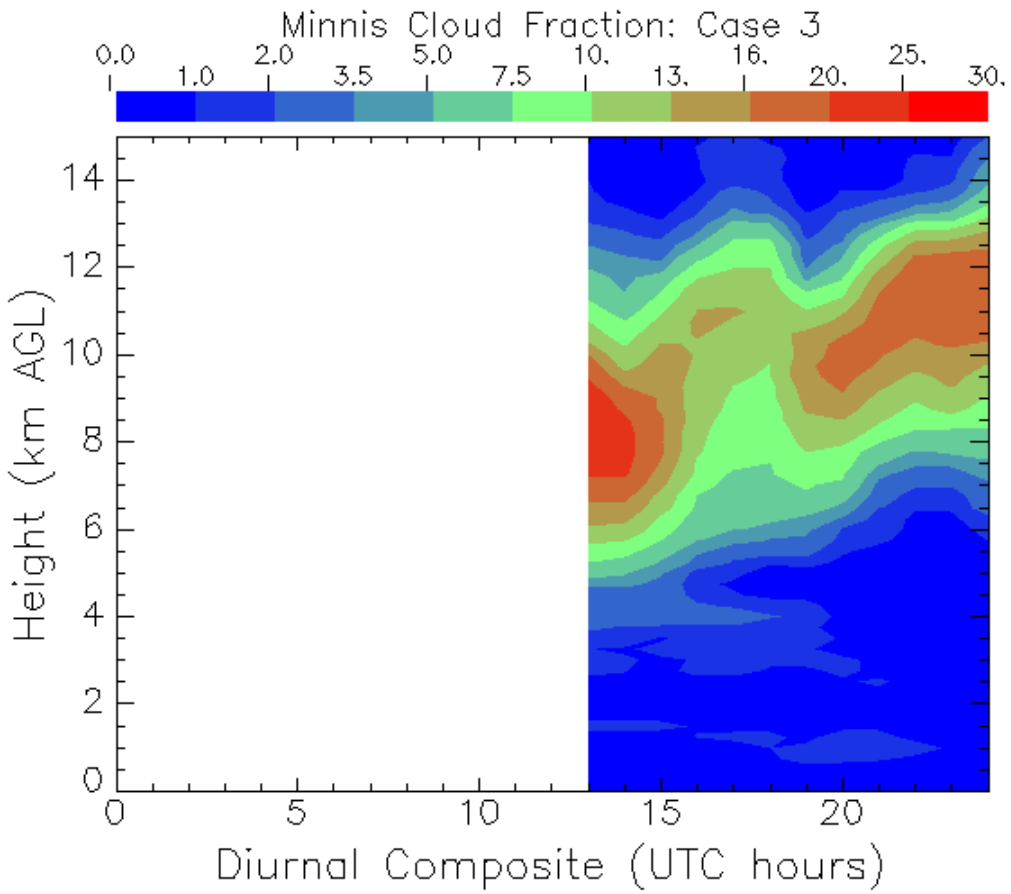

Figure 8. Cloud fraction derived from satellite cloud layer analyses, averaged by time of day over the entire CART site during the Summer 1997 SCM IOP.

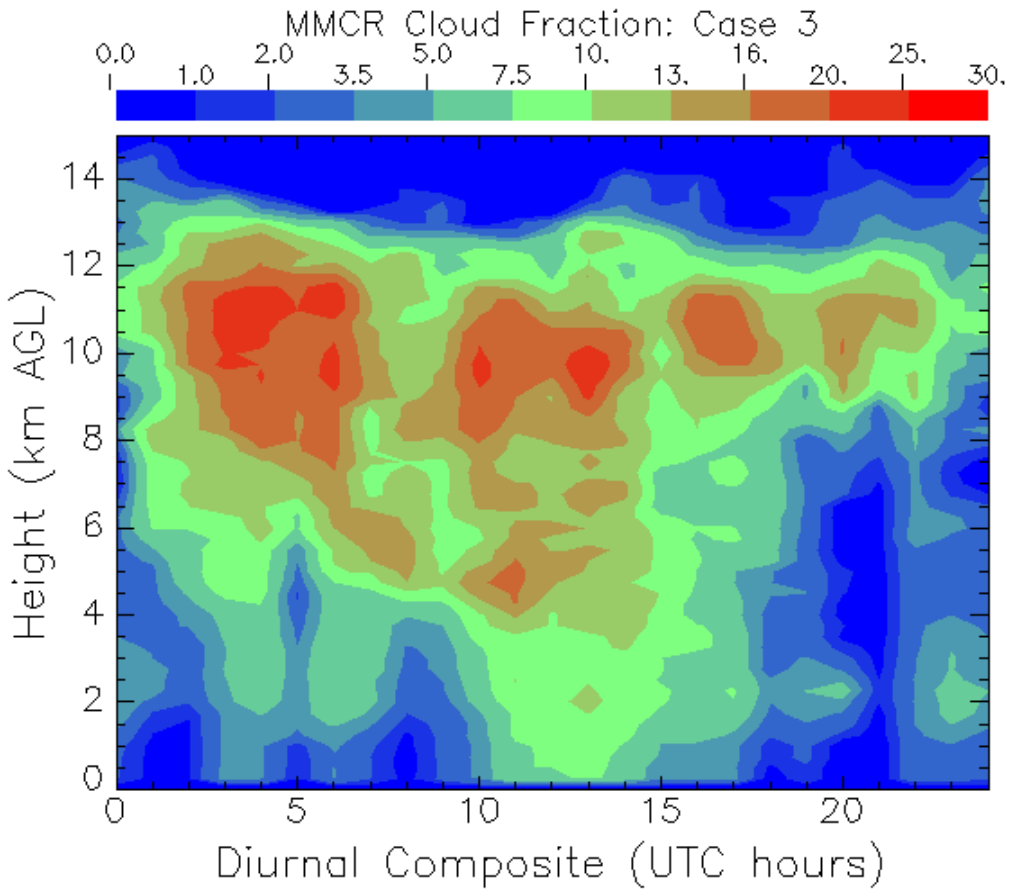

Figure 9. Cloud fractions derived from MMCR cloud occurrence frequencies during the Case 3 SCM IOP.